

Ultra-Shallow Junction Formation by $B_{18}H_{22}$ Ion Implantation

Y. Kawasaki, T. Kuroi, T. Yamashita, K. Horita, T. Hayashi, M. Ishibashi, M. Togawa* Y. Ohno and M. Yoneda
Renesas Technology Corp., 4-1 Mizuhara, Itami, Hyogo, 664-8641, Japan

*Renesas Semiconductor Engineering Corp., 4-1 Mizuhara, Itami, Hyogo, 664-8641, Japan

Tom Horsky, Dale Jacobson, and Wade Krull
SemEquip, Inc., 34 Sullivan Road, Suite 21, Billerica, MA, 01862, USA

Abstract- We have investigated Boron Cluster Implantation for ultra-shallow junction formation in transistors with gate lengths of ~60 nm. The use of large boron containing clusters is more advantageous than B^+ or BF_2^+ implantation from the viewpoint of throughput and energy contamination. Ion implantation of $B_{18}H_X^+$ cluster ions, produced by ionizing $B_{18}H_{22}$ (octadecaborane) vapor, was employed to fabricate the p-type SDE (source/drain extensions) of pMOSFETs. $B_{18}H_X^+$ implants with the energy and dose adjusted to produce equivalent projected range and B concentration as compared to conventional B^+ implants were carried out using a traditional implanter retrofitted with a SemEquip ClusterIon[®] Source. The results on blank wafers and transistor performance on test pattern wafers were compared to standard monomer B^+ implants.

Analysis of the blank wafers indicated that $B_{18}H_X^+$ showed the same or better characteristics than B^+ in junction depth and sheet resistance. Post-processing electrical measurements of the pMOSFETs implanted with $B_{18}H_X^+$ showed that they performed with nearly identical characteristics as ones implanted with B^+ .

I. INTRODUCTION

Boron ion implantation at ultra-low energies has traditionally been used for SDE formation in pMOSFETs. However, to attain production-worthy throughput, it is necessary to utilize the deceleration-mode of the implant tool. This enhances the throughput by approximately a factor of three, but results in high-energy contamination of the ion beam due to neutrals.

Boron Cluster Implantation allows for extraction and transport of ion beams at much higher energies than the desired implant energy, and has been proposed as a solution to the issues of throughput and energy contamination. Boron Cluster Implantation has been investigated using source materials such as $B_{10}H_{14}$ (decaborane) for many years[1-4]. Recently the beam current of novel $B_{18}H_X$ cluster ions from $B_{18}H_{22}$ using the SemEquip ClusterIon[®] Source has been substantially improved and it has become practical to use this cluster for the formation of ultra-shallow p-type SDE junctions.

In this work we used $B_{18}H_X^+$ implantation to fabricate the SDE of pMOSFETs with gate lengths of

~60nm. We compared results of $B_{18}H_X^+$ and B^+ from the viewpoint of transistor performance. The implants were performed at equivalent process energies corresponding to boron energies of less than 1 keV. The beams were generated in an Axcelis GSD100 ion implanter retrofitted with a SemEquip ClusterIon[®] Source and vaporizer. The original boron beam current specification for the tool was only 1 mA at 10 keV. With the ClusterIon[®] Source the tool delivers 4 mA of B at 500 eV to the wafer. Additionally the sheet resistance and boron profiles of implants into blank wafers were compared and evaluated.

II. EXPERIMENTAL

A. Mass Spectrum of $B_{18}H_{22}$

For Boron Cluster Implantation, the beam was generated from solid $B_{18}H_{22}$. Figure 1 shows the mass spectrum of the cluster beam with an extraction voltage of 10 kV. The $B_{18}H_X^+$ ($X \leq 22$) distribution ranges from about 200 to 220 AMU. This indicates that a wide variety of boron cluster ions including both mass 10 and mass 11 isotopes of boron and different numbers of hydrogen atoms remaining bonded to the borohydride molecule are contained in the mass spectrum.

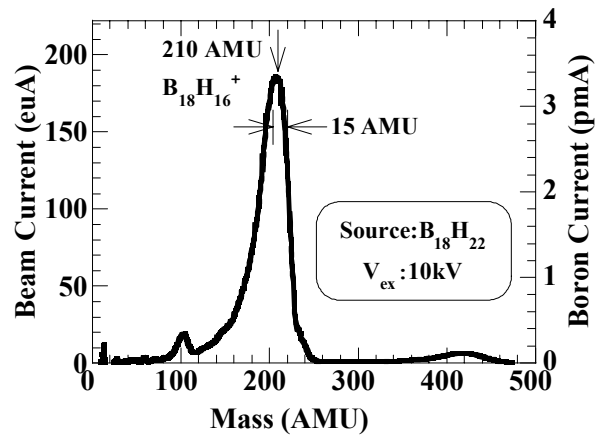


Fig.1. Mass spectrum of $B_{18}H_{22}$. The peak at mass 210 is from 18 B atoms with an average mass of 10.8 and 16 H atoms remaining attached to the octadecaborane molecule.

The peak of the distribution is located at 210 AMU or $B_{18}H_{16}^+$. From the viewpoint of beam current and

throughput, it is most advantageous to allow ~ 15 AMU, centered at mass 210, to pass through the mass defining aperture. This insures that all of the ions passed contain 18 B atoms, thereby excluding all $B_{17}H_X^+$ ions. These conditions allow 89% of the $B_{18}H_X$ ions to be utilized.

B. SIMS Profile of Boron Cluster Implantation

With the beam optimized at a mass of 210 AMU, implantations were performed at 0.5 keV equivalent energy, with a process equivalent dose of 3×10^{14} B/cm². This corresponds to extraction voltage of 10 kV with an electrical dose of 1.67×10^{13} /cm². Figure 2 shows the SIMS profile of boron in an as-implanted wafer. It can be seen that in addition to ¹¹B, ¹⁰B also was implanted. The ¹⁰B dose calculated from the profile is 20% of the total dose and ¹¹B is 80%, as expected from the natural abundance of ¹⁰B and ¹¹B.

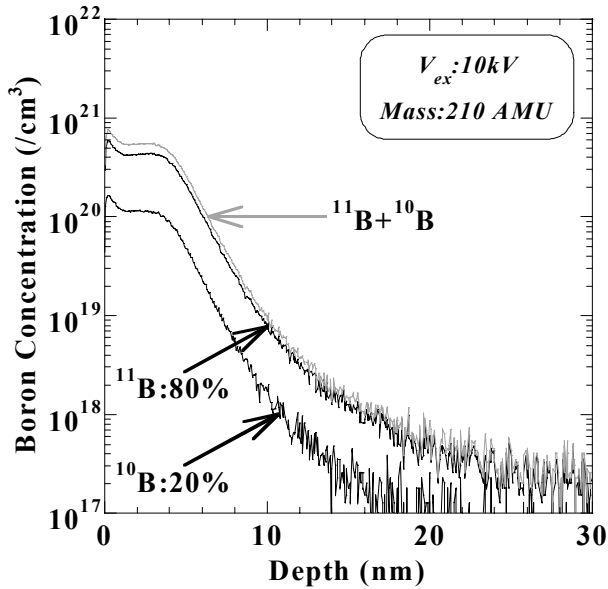


Fig.2 Typical SIMS ¹⁰B and ¹¹B depth profiles of as-implanted Si wafers. The implants were done with a $B_{18}H_X^+$ beam extracted at 10 kV (0.5 keV equivalent implant energy). The composite profile was obtained by a linear sum of the ¹⁰B and ¹¹B profiles.

C. Process Sequence of pMOSFET Fabrication

Figure 3 shows a process sequence of pMOSFET fabrication. After the gate electrode formation, either $B_{18}H_X^+$ or B^+ was implanted into SDE region with equivalent process energy, dose, and wafer orientation.

Monomer B^+ was implanted at energies of 0.2 keV, 0.5 keV, or 0.8 keV. The B^+ beam was produced from mass 11 isotopically enriched BF_3 source gas in a Bernas ion source. All implants were performed in drift mode except the 0.2keV implant which was done using the deceleration-mode with an extraction voltage of 1 kV. The implant dose was 3×10^{14} /cm²; the tilt and twist angle

were fixed at 0 degrees.

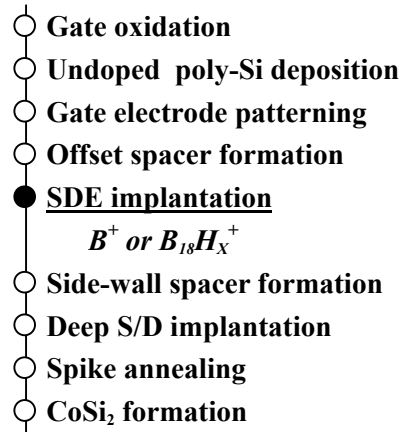


Fig.3 Process flow of pMOSFET fabrication.

$B_{18}H_X^+$ was implanted at 4 keV, 10 keV, or 16 keV equivalent to each B^+ implantation respectively with the tilt and twist angle of 0 degrees. These conditions are expected to have the same projected range as B^+ implants. The dose of each $B_{18}H_X^+$ implant was adjusted to match the dose of B^+ implants utilizing SIMS profile data that was all obtained during the same SIMS run. With these $B_{18}H_X^+$ implants the mass 10 and 11 profiles were added to obtain the total B dose, as is illustrated in Fig.2.

After side-wall spacer formation and B^+ implantation for deep source/drain (S/D) including gate electrode, spike annealing was accomplished at 1050C with a rapid ramp rate using lamp-based equipment.

III. Results and Discussions

A. Fundamental Characteristics in Blank Wafers

To evaluate the fundamental characteristics of $B_{18}H_X^+$, blank wafers were loaded in the same batch as the device wafers as described in the previous section. The implanted blank wafers also received an identical spike anneal of 1050C.

Figure 4 shows boron profiles for a 10 keV (0.5 keV process equivalent) $B_{18}H_X^+$ implant and a 0.5 keV B^+ implant both before and after annealing. The profile of $B_{18}H_X^+$ is plotted as the sum of ¹¹B and ¹⁰B, while B^+ implant is only ¹¹B. The ¹⁰B of the monomer implant can be neglected because the BF_3 is ¹¹B enriched.

The as-implanted $B_{18}H_X^+$ profile is steeper and shallower than the profile of B^+ . It is thought that this is due to the auto amorphization caused by the large boron cluster. Once the substrate crystal becomes amorphous, ion channeling is no longer possible, thus reducing the channeling tail in the B distribution.

During annealing, boron redistribution occurs, due to the high thermal budget, for both $B_{18}H_X^+$ and B^+ implants. However the B profile from the $B_{18}H_X^+$ implants is shallower than from B^+ implant.

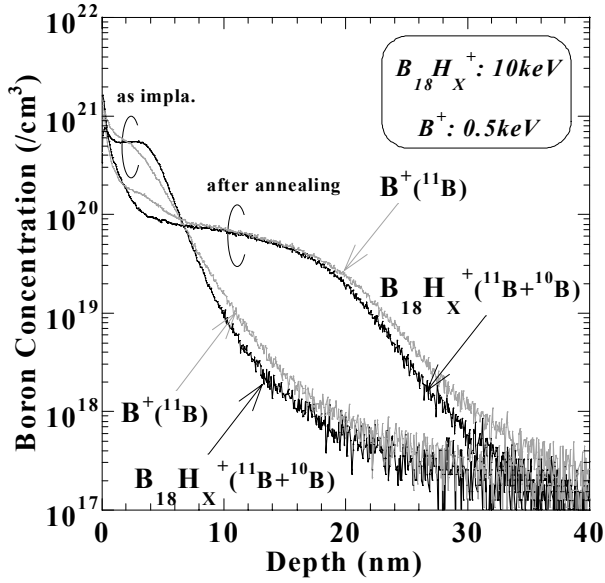


Fig.4 SIMS profiles of boron, before and after annealing of $B_{18}H_X^+$ at 10 keV and B^+ at 0.5 keV.

The boron depth for each condition is summarized in Figure 5. The depth is defined as the distance below the surface where the concentration of B is $1 \times 10^{18}/\text{cm}^3$ as measured by SIMS. The energy of the $B_{18}H_X^+$ implantation is converted to the equivalent process energy and is identical to the B^+ implant energies. In the case of $B_{18}H_X^+$ the mass 10 and 11 profiles were added, as described earlier.

The as-implanted depths from $B_{18}H_X^+$ implants are shallower than from B^+ monomer implants at all three energies. As the implant energies decrease, the depth of $B_{18}H_X^+$ and B^+ implants decreases as expected. The only exception is for the 0.2 keV B^+ implant, which was done in deceleration-mode, where energy contamination causes the B profile to be extended on the high-energy side of the distribution thus pushing out the depth.

The diffusion lengths of $B_{18}H_X^+$ are similar to B^+ diffusion lengths after annealing except for the 0.2 keV implants. This inconsistency at 0.2 keV is not yet understood, however we are currently engaged in a research project to understand this result. Nonetheless all annealed $B_{18}H_X^+$ implants have shallower junction depths than B^+ implants at equivalent energies and doses.

Figure 6 is a R_s vs. X_j plot for both $B_{18}H_X^+$ and B^+ implants at 0.2 keV, 0.5 keV, and 0.8 keV process equivalent energies after annealing. The junction depths are from Fig 5. The sheet resistance data were obtained from four-point probe measurements.

The $B_{18}H_X^+$ data and B^+ data are co-linear. This indicates that the carrier concentration of Si implanted with $B_{18}H_X^+$ is nearly identical to that of Si implanted with B^+ at process equivalent energies and doses.

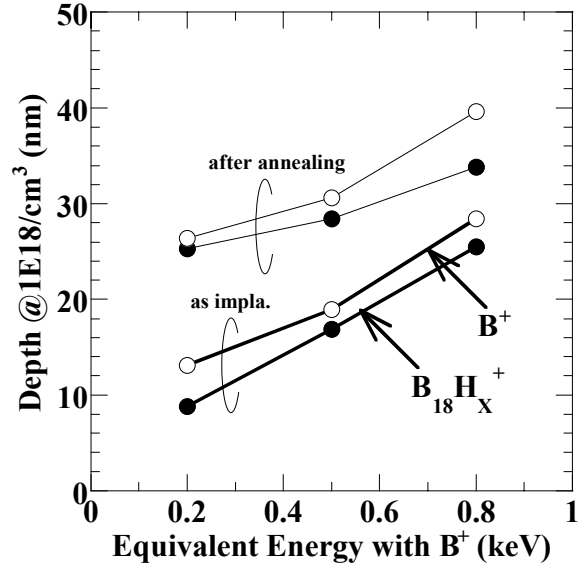


Fig.5 Junction depth of boron at $1E18/\text{cm}^3$ in the SIMS profiles, as-implanted and after annealing.

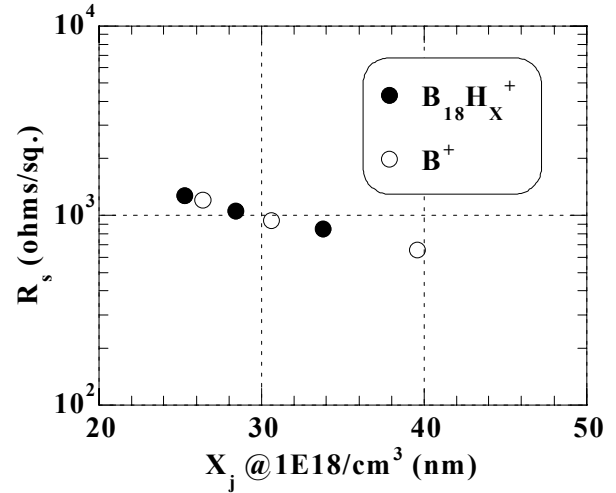


Fig.6 Junction depth and sheet resistance.

B. Transistor Characteristics

Figure 7 shows roll-off characteristics of V_{th} in the saturation region of pMOSFETs implanted with process equivalent energies and doses of either $B_{18}H_X^+$ or B^+ . In general the roll-off characteristics are very similar. However the short channel effect in these pMOSFETs can be improved by lowering the energy from 0.8 keV to 0.2 keV for both types of implants. The shift of the curve with the lowering of energy of the $B_{18}H_X^+$ implant is a little smaller than that of B^+ . This tendency is consistent with the shift of the depth between $B_{18}H_X^+$ and B^+ as shown in Fig.5.

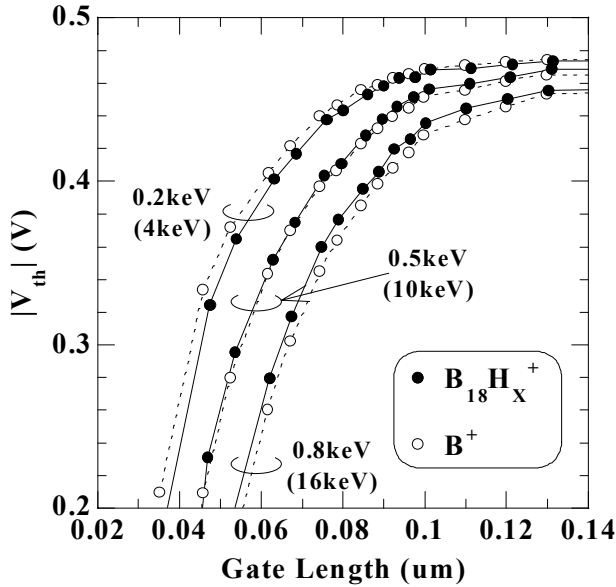


Fig.7 Dependence of $V_{th(sat)}$ on gate length.

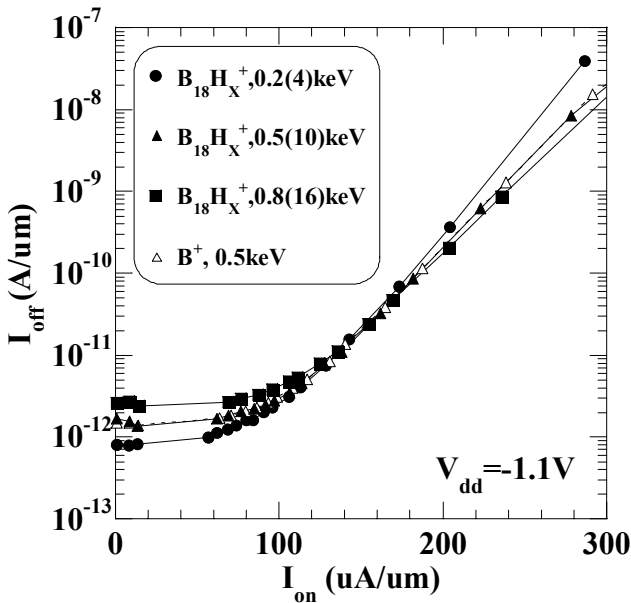


Fig.8 I_{on} - I_{off} characteristics at $V_{dd}=-1.1V$.

Figure 8 shows I_{on} - I_{off} characteristics at 1.1V for transistors implanted with $B_{18}H_X^+$ at 0.2 keV, 0.5 keV, or 0.8 keV equivalent energies, or with B^+ at 0.5 keV. The I_{on} - I_{off} curve of $B_{18}H_X^+$ at 0.5 keV has the same characteristics as that of B^+ implant at an equivalent energy. It can be seen that the drain current of $B_{18}H_X^+$ and B^+ implanted transistors are the same at the off-state leakage current of 20 pA/um, though I_{on} - I_{off} curves of $B_{18}H_X^+$ are different from each other on the whole.

IV. Summary

The fabrication of pMOSFET devices with gate lengths of ~ 60 nm utilizing $B_{18}H_X^+$ cluster ion implantation for the formation of the source/drain extensions has been successfully demonstrated.

Using a traditional ion implanter retrofitted with a SemEquip ClusterIon[®] Source and vaporizer to form the p-type SDE, split lot tests have shown that pMOSFETs fabricated with this new, unique and revolutionary implant material have transistor performance equal to transistors produced using traditional monomer B^+ implants.

It has been verified that $B_{18}H_X^+$ implantation can be used to produce ultra-shallow junctions for MOSFET fabrication at production-worthy throughputs.

References

- [1] K. Goto et al., IEDM(1996) pp435-438
- [2] D.C. Jacobson et al., IIT(2000) pp300-303
- [3] A. Perel et al., IIT(2000) pp304-307
- [4] S. Umisedo et al., IWJT(2004) pp27-30